Article

Structural and Electrical Properties of Atomic Layer Deposited PtRu Bimetallic Alloy Thin Films

Hyun-Jae Woo [1,†], Woo-Jae Lee [1,†], Chang-Min Kim [1], Qimin Wang [2], Shihong Zhang [3], Yong-Jin Yoon [4,*] and Se-Hun Kwon [1,*]

[1] School of Materials Science and Engineering, Pusan National University, Busan 46241, Korea; present_w@naver.com (H.-J.W.); woojl@pusan.ac.kr (W.-J.L.); changmin.kim0317@gmail.com (C.-M.K.)
[2] School of Electromechanical Engineering, Guangdong University of Technology, Guangzhou 510006, China; qmwang@gdut.edu.cn
[3] School of Materials Science and Engineering, Anhui University of Technology, Maanshan 243002, China; tougaoyouxiang206@163.com
[4] Department of Mechanical Engineering, Korea Advanced Institute of Science and Technology, 291 Daehak-ro, Yuseong-gu, Daejeon 34141, Korea
[*] Correspondence: yongjiny@kaist.ac.kr (Y.-J.Y.); sehun@pusan.ac.kr (S.-H.K.)
[†] These authors contributed equally to this work.

Abstract: The structural and electrical properties of PtRu bimetallic alloy (BA) thin films prepared via atomic layer deposition (ALD) were systemically investigated according to the film composition, which was controlled at a deposition temperature of 340 °C by changing the numbers of Pt and Ru subcycles of a supercycle. As-deposited PtRu BA thin films exhibited weaker crystallinity than $Pt_{36}Ru_{64}$ when the Ru content was high. However, crystallinity improved, and the peak shifts became clearer after Ar heat treatment at 700 °C, reflecting the formation of well-mixed solid solutions. The electrical resistivity and work function also improved. The work function of PtRu BA thin films can be controlled between the work functions of Pt and Ru, and is only weakly dependent on the film composition in the single solid solution region.

Keywords: PtRu bimetallic alloy; atomic layer deposition; thin films; electrical properties; structural properties

1. Introduction

Bimetallic alloy (BA) systems allow researchers to discover new properties, or tune existing ones, by changing the nature or proportions of the two elements [1–5]. Unlike single metals, two different metals combined in BAs can exhibit synergistic behaviors. Of the various BA systems, the PtRu system has recently been used to enhance and/or tune mechanical [2], catalytic [5–7], and electrical properties [8–10]. Various PtRu BAs (bulk, nanoparticles, nanowires, and thin films) have been studied using solution- or vapor-based methods [2,5–9]. To date, however, most studies have focused on the catalytic performance of PtRu BA nanoparticles. The equilibrium bulk phase diagram of a Pt-Ru binary system [11] revealed that Pt and Ru can form a very wide range of solid solutions with a face-centered cubic (FCC) structural component of up to ~60 at.% Ru. Additionally, the metals can form solid solutions with a hexagonal close-packed (HCP) structural component above ~84 at.% Ru. Both (FCC and HCP) solid solution phases can coexist between ~60 at.% and ~84 at.% Ru at 500 °C. The broad range over which single FCC and HCP solid solution phases can exist in Pt-Ru binary systems facilitates tuning of electrical resistivity and work function. Changes in the electronic resistivities, work functions, and the crystal structures of ultra-high vacuum (UHV)-sputtered PtRu BA thin films of various compositions matched the predictions of the equilibrium bulk phase diagram. Additionally, the work functions

of single FCC and HCP solid solution phases were only weakly dependent on the compositions [8]. Therefore, it allows for a proper material design to obtain similar electrical properties with reduced Pt content.

Recently, atomic layer deposition (ALD) has received extensive attention. Both film thickness and composition can be precisely controlled; uniform coverage of even large complex three-dimensional surfaces is possible [7,9,10]. With these advantages, ALD has emerged as a useful tool to prepare PtRu BAs for various applications, such as electrode materials for electronic devices [9,10], as well as electrocatalysts [7,12,13]. However, a comprehensive analysis of the electrical properties of ALD PtRu BA thin films according to film composition has rarely been reported.

Therefore, we herein investigated PtRu BA thin films prepared via ALD, and used a supercycle to control film composition. The relationship between crystal structure, electrical resistivity, and work function depending on the composition was carefully investigated, and the effect of Ar heat treatment on those properties was systemically discussed.

2. Materials and Methods

Prior to deposition, SiO_2 (300 nm)/Si (100) substrates were cleaned via sequential ultrasonication in acetone, isopropyl alcohol (IPA), and deionized (DI) water for 10 min in each step to remove any hydrocarbons, and then dried under high-purity nitrogen. Considering the overlapping ALD temperature window of both ALD-Pt and ALD-Ru (Figure S1), PtRu BA thin films were deposited on these substrates at 340 °C under 1 Torr. The supercycle consisted of two groups of subcycles allocated to the Ru deposition and Pt deposition, respectively. Within a supercycle, the Pt subcycle involved injection of dimethyl(N,N-dimethyl-3-butene-1-amine-N)platinum (DDAP; Tanaka Kikinzoku Kogyo, Tokyo, Japan) in 100 sccm Ar for 10 s, a purge injection of 100 sccm Ar for 20 s, an injection of O_2 (50 sccm) for 10 s, and another 100 sccm Ar purge injection for 20 s. An Ru subcycle consisted of an injection of dicarbonyl-bis(5-methyl-2,4-hexanediketonato)Ru(II) (Carish; Tanaka Kikinzoku Kogyo) in 100 sccm Ar for 15 s, a purge injection of 100 sccm Ar for 20 s, an injection of O_2 (50 sccm) for 10 s, and another 100 sccm Ar purge injection for 20 s. To ensure an adequate supply of precursors, DDAP and Carish were maintained in stainless-steel canisters at 60 °C and 75 °C, respectively. Additionally, ultra-high purity (UHP) Ar (99.999%) and O_2 (99.999%) were used as carrier and reactant gases. To control the relative proportions of Pt and Ru, the numbers of Pt and Ru subcycles were varied (Table 1). However, the number of supercycles was chosen to ensure that the final films were ~30-nm-thick, regardless of composition. We aimed to reduce/eliminate any effect of film thickness on the structural and electrical properties of PtRu BA thin films. After deposition of the films, rapid thermal annealing (RTA; GVRTAS-9100) was performed at 700 °C under 1 Torr of Ar for 10 min to improve crystallinity, and to mix the thin films by redistributing the dopant atoms.

Table 1. A supercycle design and corresponding compositions for PtRu bimetallic alloy thin films.

Pt:Ru Subcycle Ratio in a Supercycle	Compositions
Pt:Ru = 1:10	$Pt_{11}Ru_{89}$
Pt:Ru = 1:5	$Pt_{18}Ru_{82}$
Pt:Ru = 1:1	$Pt_{36}Ru_{64}$
Pt:Ru = 5:1	$Pt_{70}Ru_{30}$
Pt:Ru = 10:1	$Pt_{84}Ru_{16}$

Film thickness was measured by field-emission scanning electron microscopy (FE-SEM; S-4800; Hitachi, Tokyo, Japan). The crystal structure was investigated by X-ray diffraction (XRD; Ultima IV; Rigaku, Tokyo, Japan) using 1.54 Å Cu-Kα radiation. Film compositions were analyzed with Auger electron spectroscopy (AES; SAM 4300; PerkinElmer, Waltham, MA, USA), and calibrated by Rutherford back-scattering (RBS; NEC-3SDH; National Electrostatics Corporation, Middleton, WI, USA). In terms of electrical properties, electrical

resistivity was calculated from the sheet resistance measured by a four-point probe (CMT-SR2000N; Advanced Instrument Technologies, Austin, TX, USA) at a defined film thickness. The work functions of the films were determined via Kelvin probe force microscopy (KPFM; MFP-3D; Oxford Instruments Asylum Research, Santa Barbara, CA, USA), using the measured contact potential difference (CPD) method. The KPFM method was described in detail previously [10].

3. Results and Discussion

Prior to thin film deposition, the self-limiting growth of ALD-Pt and -Ru thin films was studied at 340 °C under 1 Torr. Figure 1a shows that the growth rate of Pt thin films depended on the DDAP pulse time to confirm the ALD reaction mechanism. When the DDAP pulse time increased from 5 to 15 s, the growth rate increased, and then saturated at 0.08 nm/cycle above 10 s. Next, the growth rate of Ru thin films was investigated as a function of the Carish pulse time (Figure 1b). As the pulse time increased from 7 to 30 s, similar saturation behaviors were observed above 15 s. The saturated growth rate of the ALD-Ru process was 0.091 nm/cycle. Thus, both Pt and Ru thin films were successfully deposited using a typical self-limiting ALD reaction mechanism. All sequences other than the precursor pulse time (DDAP or Carish) were fixed (as described in the Materials and Methods).
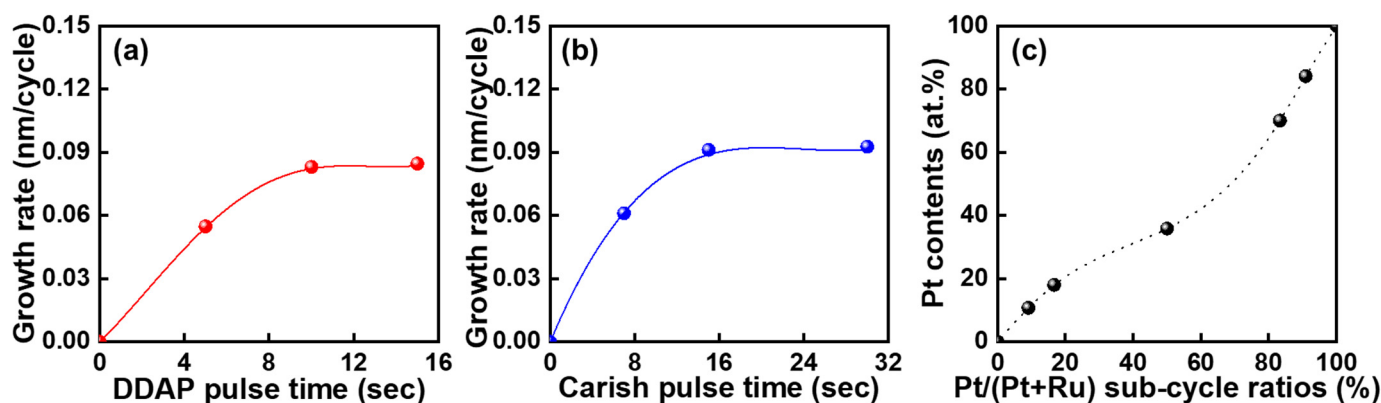

Figure 1. Growth rate of (**a**) ALD-Pt depending on the DDAP pulse time, and (**b**) ALD-Ru depending on the Carish pulse time at a deposition temperature of 340 °C. In addition, (**c**) compositions of the PtRu bimetallic alloy thin films depending on the Pt/(Pt + Ru) subcycle ratios (%).

In order to control the thin film compositions, different supercycles were applied as described in Table 1. The Pt:Ru subcycle ratios were 1:10, 1:5, 1:1, 5:1, and 10:1. The number of supercycles was controlled to ensure that all films were about 30-nm-thick. Film compositions were then analyzed by AES and RBS. Figure 1c shows that the film compositions can be simply controlled by varying the Pt:Ru subcycle ratio. The resultant compositions were $Pt_{11}Ru_{89}$, $Pt_{18}Ru_{82}$, $Pt_{36}Ru_{64}$, $Pt_{70}Ru_{30}$, and $Pt_{84}Ru_{16}$ for Pt:Ru subcycle ratios of 1:10, 1:5, 1:1, 5:1, and 10:1, respectively. Due to the difference in saturated growth rate between ALD-Pt and -Ru, the changes in compositions were non-linear.

The microstructures of as-deposited ALD-PtRu BA thin films depending on the film composition were analyzed by XRD, as shown in Figure 2a. It is worth mentioning again that Pt-Ru binary system has a single FCC solid solution phase up to ~60 at.% Ru and a single HCP solid solution phase above ~84 at.% Ru, and those two (FCC and HCP) solid solution phases can coexist between ~60 at.% and ~84 at.% Ru at 500 °C according to the equilibrium bulk phase diagram [11], as described in the introduction. Figure 2a shows that the as-deposited Pt thin films had a typical FCC structure with (111), (200), and (220) planes. As-deposited Ru thin films exhibited an HCP structure with (100), (002), and (101) planes. However, the behaviors of as-deposited PtRu BA thin films differed somewhat from those predicted by the equilibrium bulk phase diagram. With increasing Ru component

up to 30 at.%, the Pt (111) peaks clearly shifted to higher angles, which indicates a smaller Ru atom substituted into the FCC Pt lattice [8]. Thus, $Pt_{84}Ru_{16}$ and $Pt_{70}Ru_{30}$ BA thin films showed a good agreement with a bulk phase diagram, where a single FCC solid solution phase exists. However, the PtRu BA thin films with higher Ru contents than 30 at.%—such as $Pt_{36}Ru_{64}$, $Pt_{18}Ru_{82}$, and $Pt_{11}Ru_{89}$—exhibited relatively weak peak intensities. Moreover, $Pt_{36}Ru_{64}$ and $Pt_{18}Ru_{82}$ only exhibited a weak solid solution phase, where the co-existence of FCC and HCP solid solution is to be expected [8,11]. Furthermore, it was difficult to distinguish the phases for the $Pt_{11}Ru_{89}$ sample. Therefore, to prepare well-mixed PtRu BA thin films and improve the film crystallinity, the samples were subjected to Ar heat treatment at 700 °C under 1 Torr. Figure 2b demonstrates the effect of Ar heat treatment on the microstructures of PtRu BA thin films. After Ar heat treatment, a further crystallization of PtRu BA thin films was observed. In particular, $Pt_{18}Ru_{82}$ BA thin films exhibited both FCC and HCP solid solution phases, which was not observed in the as-deposited samples. To quantitatively analyze the degree of peak shifts, we derived the peak position of Pt (111) and Ru (002) before and after Ar heat treatment, as illustrated in Figure 2c. It was noted that the Pt (111) peak position shifted to a higher angle after Ar heat treatment with increasing Ru content up to 64 at.%. On the other hand, Ru (002) shifted to the lower angle after Ar heat treatment, with increasing Pt content up to 18 at.%. Thus, Ar heat treatment facilitated the formation of well-mixed PtRu BA thin films, and the atoms were redistributed.
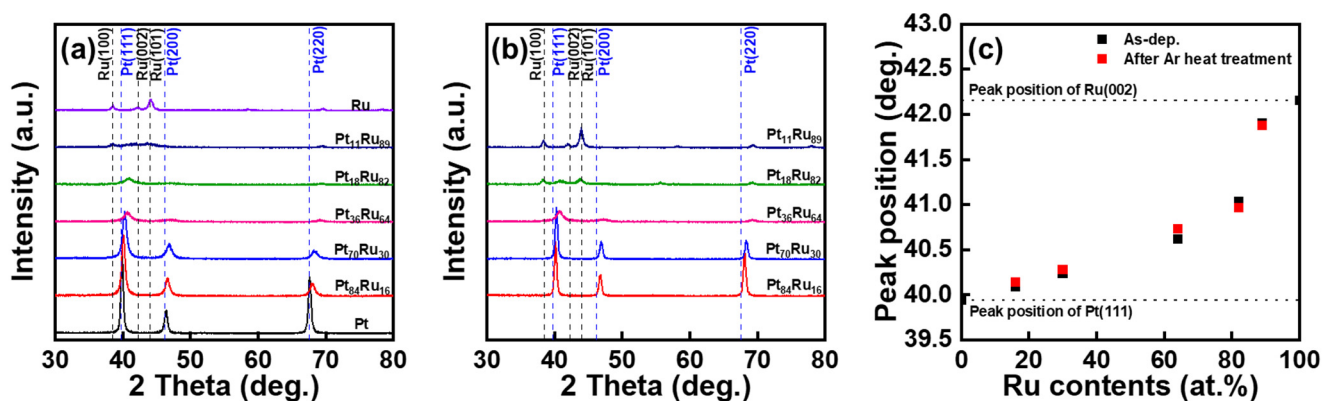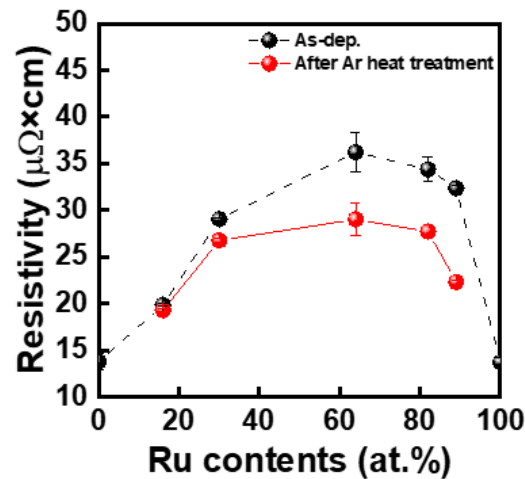

Figure 2. XRD patterns of PtRu bimetallic alloy thin films according to the film compositions (**a**) before, and (**b**) after Ar heat treatment at 700 °C under 1 Torr. (**c**) The peak positions of Pt (111) and Ru (002) before and after Ar heat treatment.

Next, we analyzed electrical resistivity (Figure 3). The resistivities of the pure Pt and Ru thin films were 13.71 and 13.79 μΩ·cm, respectively. As the Ru content of PtRu BA films increased, the resistivity increased from 19.8 μΩ·cm ($Pt_{84}Ru_{16}$) to 36.2 μΩ·cm ($Pt_{36}Ru_{64}$). As the Ru content increased further (from $Pt_{36}Ru_{64}$ to $Pt_{11}Ru_{89}$), the resistivity gradually decreased from 36.2 to 32.4 μΩ·cm. Compared to Pt-rich PtRu BA thin films, Ru-rich thin films exhibited higher resistivity, attributable to Pt alloying, and reflecting the weak crystalline structures of as-deposited Ru-rich PtRu BA thin films. However, after Ar heat treatment, resistivity improved. Pt-rich PtRu BA thin films ($Pt_{84}Ru_{16}$ and $Pt_{70}Ru_{30}$) did not show sudden decreases in resistivity. However, as the Ru content increased, resistivity greatly improved after Ar heat treatment. Thus, the highest electrical resistivity of Ar heat treated PtRu BA thin film was about 29 μΩ·cm for $Pt_{36}Ru_{64}$ within our experiments. These results are in good agreement with the XRD data, i.e., Ar heat treatment enhanced crystallization. Although the resistivity values were not reported, a similar change in the resistivity depending on the film composition was also described in the sputtered PtRu BA thin films [8]. For the sputtered PtRu alloy thin films, the decrease in the resistivity was also attributed to the Ar +3% H_2 heat treatment. The changes in the resistivity of the single-phase solid solution regions of Ar heat treated ALD-PtRu BA thin films were well explained by the well-known Nordheim rule, which is applicable to single-phase

homogeneous solid solution alloys. The effect of solute atoms on electrical resistivity can be expressed as follows [14]:

$$\rho_{\text{solute atom}} = CX(1 - X) \tag{1}$$

where $\rho_{\text{solute atom}}$ is the resistivity attributable to electron scattering from solute atoms, C is the Nordheim coefficient, and X is the atomic fraction of solute atoms in the solid solution.

Figure 3. Electrical resistivity of PtRu bimetallic alloy thin films according to the film compositions before and after Ar heat treatment at 700 °C.

The effects of film composition on the work functions of the thin films were analyzed by KFPM (Figure 4). The as-deposited Pt and Ru film work functions were about 5.4 and 4.97 eV, respectively. The work functions of the PtRu BA thin films ranged between these values. In the single FCC solid solution phase region, the work functions gradually decreased with increasing Ru content. A similar gradual decrease was observed in the single HCP solid solution phase region. A relatively drastic difference in work function was observed between $Pt_{36}Ru_{64}$ and $Pt_{18}Ru_{82}$, in which two solid solution phases co-exist. Such behavior became clearer after Ar heat treatment due to the formation of well-mixed PtRu BA thin films. A similar change in the work functions was also observed for the sputtered PtRu BA thin films.
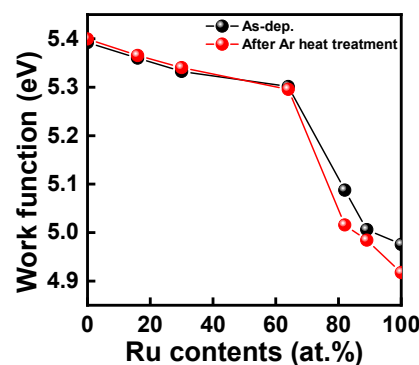
Figure 4. Work functions of PtRu bimetallic alloy thin films according to the film compositions before and after Ar heat treatment at 700 °C.

4. Conclusions

By varying the number of Pt and Ru subcycles in a supercycle, the composition of PtRu BA thin films was precisely controlled from $Pt_{11}Ru_{89}$ to $Pt_{84}Ru_{16}$. The microstructures and electrical properties of the ALD-PtRu BA thin films were carefully investigated before and after Ar heat treatment. As-deposited PtRu BA thin films exhibited weak crystallinity when the Ru content was higher. After Ar heat treatment, crystallinity improved, and the

peak shifts became clearer, attributable to the formation of well-mixed solid solutions (as expected from the bulk phase diagram). Ar heat treatment improved the electrical resistivity and work function by mixing the thin films and enhancing crystallinity. Consequently, the electrical resistivity of the single-phase solid solution regions of Ar heat treated ALD-PtRu BA thin films followed the Nordheim rule, and within our experiments the highest electrical resistivity of about 29 μΩ·cm was obtained for Ar heat treated $Pt_{36}Ru_{64}$. The work functions of Ar heat treated ALD-PtRu BA thin films exhibited a gradual change in a single solid solution phase region, and a drastic change in the regions where two solid solution phases co-exist.

Supplementary Materials: The following supporting information can be downloaded at: https://www.mdpi.com/article/10.3390/coatings12010101/s1, Figure S1: The growth rate and resistivity of ALD-Ru thin films using Carish precursor as a function of the deposition temperature.

Author Contributions: Conceptualization, Y.-J.Y. and S.-H.K.; methodology, Q.W., S.Z. and S.-H.K.; investigation, H.-J.W. and W.-J.L.; data curation, H.-J.W. and C.-M.K.; writing—original draft preparation, H.-J.W. and W.-J.L.; writing—review and editing, Y.-J.Y. and S.-H.K.; visualization, H.-J.W.; supervision, Y.-J.Y. and S.-H.K.; project administration, S.-H.K.; funding acquisition, S.-H.K. All authors have read and agreed to the published version of the manuscript.

Institutional Review Board Statement: Not applicable.

Informed Consent Statement: Not applicable.

Data Availability Statement: Not applicable.

Conflicts of Interest: The authors declare no conflict of interest.

References

1. Kusada, K.; Kobayashi, H.; Ikeda, R.; Kubota, Y.; Takata, M.; Toh, S.; Yamamoto, T.; Matsumura, S.; Sumi, N.; Sato, K.; et al. Solid solution alloy nanoparticles of immiscible Pd and Ru elements neighboring on Rh: Changeover of the thermodynamic behavior for hydrogen storage and enhanced CO-oxidizing ability. *J. Am. Chem. Soc.* **2014**, *136*, 1864–1871. [CrossRef] [PubMed]
2. Hyun, S.; Kraft, O.; Vinci, R.P. Mechanical behavior of Pt and Pt-Ru solid solution alloy thin films. *Acta Mater.* **2004**, *52*, 4199–4211. [CrossRef]
3. Muller, J.E.; Krtil, P.; Kibler, L.A.; Jacob, T. Bimetallic alloys in action: Dynamic atomistic motifs for electrochemistry and catalysis. *Phys. Chem. Phys.* **2014**, *16*, 15029–15042. [CrossRef] [PubMed]
4. Gilroy, K.D.; Ruditskiy, A.; Peng, H.-C.; Qin, D.; Xia, Y. Bimetallic Nanocrystals: Synthesis, Properties, and Applications. *Chem. Rev.* **2016**, *116*, 10414–10427. [CrossRef] [PubMed]
5. Jin, L.; Zhang, Z.; Zhuang, Z.; Meng, Z.; Li, C.; Shen, Y. PdPt bimetallic alloy nanowires-based electrochemical sensor for sensitive detection of ascorbic acid. *RSC. Adv.* **2016**, *6*, 42008–42013. [CrossRef]
6. Zheng, J.; Cullen, D.A.; Forest, R.V.; Wittkopf, J.A.; Zhuang, Z.; Sheng, W.; Chen, J.G.; Yan, Y. Platinum−ruthenium nanotubes and platinum−ruthenium coated copper nanowires as efficient catalysts for electro-oxidation of methanol. *ACS Catal.* **2015**, *5*, 1468–1474. [CrossRef]
7. Jiang, X.; Gür, T.M.; Prinz, F.B.; Bent, S.F. Atomic layer deposition (ALD) co-deposited Pt-Ru binary and Pt skin catalysts for concentrated methanol oxidation. *Chem. Mater.* **2010**, *22*, 3024–3032. [CrossRef]
8. Todi, R.M.; Warren, A.P.; Sundaram, K.B.; Barmak, K.; Coffey, K.R. Characterization of Pt-Ru binary alloy thin films for work function tuning. *IEEE Electron Device Lett.* **2006**, *27*, 542–545. [CrossRef]
9. Pyeon, J.J.; Cho, C.J.; Jeong, D.S.; Kim, J.-S.; Kang, C.-Y.; Kim, S.K. A Ru–Pt alloy electrode to suppress leakage currents of dynamic random-access memory capacitors. *Nanotechnology* **2018**, *29*, 455202. [CrossRef] [PubMed]
10. Kim, C.-M.; Lee, W.-J.; Bera, S.; Kwon, S.-H. Effect of the film thickness on the work function of Pt-Ru bimetallic alloy films by atomic layer deposition. *J. Korean Phys. Soc.* **2019**, *75*, 1–4. [CrossRef]
11. Okamoto, H. Pt-Ru (Platinum-Ruthenium). *J. Phs. Eqil. Diff.* **2008**, *29*, 471. [CrossRef]
12. Zhang, L.; Si, R.; Liu, H.; Chen, N.; Wang, Q.; Adair, K.; Wang, Z.; Chen, J.; Song, Z.; Li, J.; et al. Atomic layer deposited Pt-Ru dual-metal dimers and identifying their active sites for hydrogen evolution reaction. *Nat. Commun.* **2019**, *10*, 4936. [CrossRef] [PubMed]

13.　Luo, W.; Gan, J.; Huang, Z.; Chen, W.; Qian, G.; Zhou, X.; Duan, X. Boosting HER performance of Pt-based catalysts immobilized on functional Vulcan carbon by atomic layer deposition. *Front. Mater.* **2019**, *6*, 251. [CrossRef]

14.　Nagarjuna, S.; Balasubramanian, K.; Sarma, D.S. Effect of Ti addition on the electrical resistivity of copper. *Mater. Sci. Eng. A* **1997**, *225*, 118–124. [CrossRef]